Strong Suppression of the Spin Hall Effect in the Spin Glass State

Y. Niimi,[1,*] M. Kimata,[1] Y. Omori,[1] B. Gu,[2]
T. Ziman,[3] S. Maekawa,[2,4] A. Fert,[5] and Y. Otani[1,6]

[1]*Institute for Solid State Physics, University of Tokyo, 5-1-5 Kashiwa-no-ha, Kashiwa, Chiba 277-8581, Japan*

[2]*Advanced Science Research Center, Japan Atomic Energy Agency, Tokai 319-1195, Japan*

[3]*CNRS and Institut Laue Langevin, Boîte Postale 156, F-38042 Grenoble Cedex 9, France*

[4]*ERATO, Japan Science and Technology Agency, Sendai 980-8577, Japan*

[5]*Unité Mixte de Physique CNRS/Thales, 91767 Palaiseau France associée à l'Université de Paris-Sud, 91405 Orsay, France*

[6]*RIKEN-CEMS, 2-1 Hirosawa, Wako, Saitama 351-0198, Japan*

(Dated: October 2, 2015)

*Electronic address: niimi@phys.sci.osaka-u.ac.jp; Present address: Department of Physics, Osaka University, Toyonaka, Osaka 560-0043, Japan

A. Sample fabrications and experimental setup

The SHE device is based on a lateral spin valve structure where CuMnBi(Ir) is inserted in between two Py wires and bridged by a Cu wire, as shown in Fig. 1(b). Samples were patterned using electron beam lithography onto a thermally oxidized silicon substrate coated with polymethyl-methacrylate (PMMA) resist for depositions of Py and Cu, or coated with ZEP 520A resist for depositions of CuMnBi and CuMnIr.

A pair of Py wires was first deposited using an electron beam evaporator under a base pressure of 10^{-9} Torr. The width and thickness of the Py wires are 100 and 30 nm, respectively. The CuMnBi(Ir) middle wire was next deposited by magnetron sputtering using a CuMnBi(Ir) target. The Bi and Ir concentrations used in this work were fixed at 0.5% and 1%, respectively, while the Mn concentration was changed from 0 to 1.5% for CuMnBi ($Cu_{99.5}Bi_{0.5}$, $Cu_{99}Mn_{0.5}Bi_{0.5}$, $Cu_{98.5}Mn_1Bi_{0.5}$, and $Cu_{98}Mn_{1.5}Bi_{0.5}$), and from 0 to 6% for CuMnIr ($Cu_{99}Ir_1$, $Cu_{98}Mn_1Ir_1$, $Cu_{96}Mn_3Ir_1$, and $Cu_{93}Mn_6Ir_1$). As a reference, we also prepared $Cu_{97}Mn_3$ SHE devices. The width and thickness of the Cu-based alloys are 250 and 20 nm, respectively. The post-baking temperature for the PMMA resist was kept below 90°C after the deposition of CuMnBi alloys since bismuth has a low melting temperature (270°C). Before deposition of a Cu bridge, we performed a careful Ar ion beam etching for 30 seconds in order to clean the surfaces of the Py and CuMnBi(Ir) middle wires. After the Ar ion etching, the device was moved to another chamber without breaking a vacuum and subsequently the Cu bridge was deposited by a Joule heating evaporator using a 99.9999% purity source. Both the width and thickness of the Cu bridge are 100 nm.

The Hall bars for AHE measurements were also prepared using electron beam lithography onto a thermally oxidized silicon substrate coated with ZEP 520A resist. The length and width of the Hall bar are 20 and 3 μm, respectively.

Both the SHE and AHE measurements have been carried out using an ac lock-in amplifier and a ^{4}He flow cryostat. The magnetization meausrements shown in Fig. 2(f) were performed with a commercial SQUID magnetometer MPMS (Quantum Design).

B. Extra data on SHEs in CuMn, CuMnBi and CuMnIr

In this section, we present some additional data which are not shown in the main text.

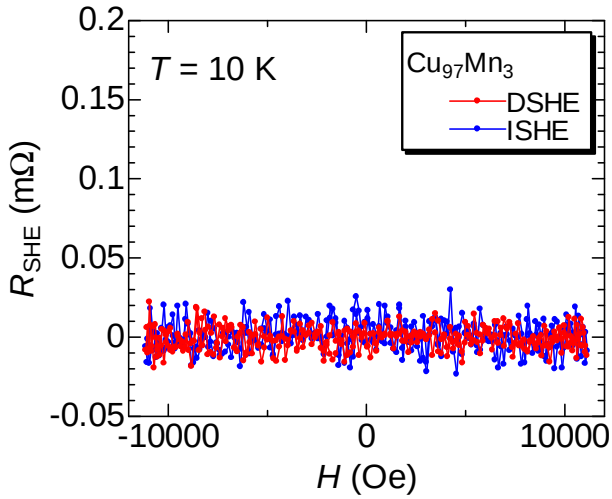

Figure S1: ISHE and DSHE in $Cu_{97}Mn_3$ measured at $T = 10$ K.

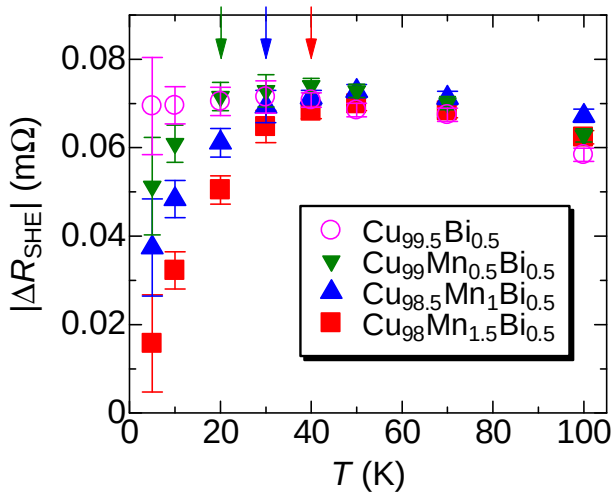

Figure S2: $|\Delta R_{\rm SHE}|$ for $Cu_{99.5-x}Mn_xBi_{0.5}$ ($x = 0$, 0.5, 1, and 1.5) alloys as a function of T. The arrows indicate T^* for each Mn concentration.

In Fig. S1, we first show the ISHE and DSHE in $Cu_{97}Mn_3$ measured with the same device structure as in Fig. 1(b). No SHE is observed in the CuMn binary alloy. Thus, an additional nonmagnetic impurity with strong spin-orbit interaction is needed to see the SHE in CuMn.

Next we show typical $|\Delta R_{\rm SHE}|$ data for four different CuMnBi alloys ($Cu_{99.5-x}Mn_xBi_{0.5}$ ($x = 0$, 0.5, 1, and 1.5)) as a function of T in Fig. S2. As already pointed out in the main text, the reduction occurs below T^* and T^* is shifted to the lower temperature side with decreasing the concentration of Mn (see the arrows in in Fig. S2). On the other hand, all

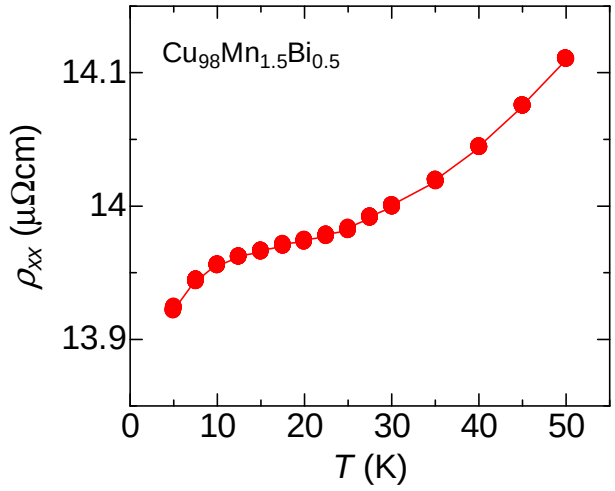

Figure S3: ρ_{xx} of $Cu_{98}Mn_{1.5}Bi_{0.5}$ as a function of T.

$|\Delta R_{\rm SHE}|$ merge together above 50 K.

In Fig. S3, ρ_{xx} of $Cu_{98}Mn_{1.5}Bi_{0.5}$ is plotted as a function of T. Unlike the case of ρ_{xx} of $Cu_{99.5}Bi_{0.5}$, it does not saturate even below 10 K but continues to decrease with decreasing T. Such a reduction was also observed for other CuMn(Bi) alloys. We note that the reduction is very small (less than 1% compared to the total resistivity) and is not enough to explain the large suppresion in $|\alpha_{\rm H}|$.

In the main text, $|\rho^{\rm 3D}_{\rm SHE}|/\rho_{\rm Bi}$ and $\lambda^{\rm 3D}_{\rm M}$ are plotted as a function of T in Fig. 3. Here we show $|\rho^{\rm 1D}_{\rm SHE}|/\rho_{\rm Bi}$ and $\lambda^{\rm 1D}_{\rm M}$ obtained with the one-dimensional (1D) spin diffusion model [12-14] in Fig. S4. Although the absolute values are slightly different, both 3D and 1D data show the same tendencies [see also Fig. 3].

Only for $Cu_{98}Mn_{1.5}Bi_{0.5}$, there is an obvious reduction in $\lambda^{\rm 3D}_{\rm M}$ (or $\lambda^{\rm 1D}_{\rm M}$). To check whether the reduction of $|\alpha^{\rm 3D}_{\rm H}|$ is dominated by $\lambda^{\rm 3D}_{\rm M}$, we have fixed $\lambda^{\rm 3D}_{\rm M}$ below $T^* = 40$ K at 41 nm and obtained $|\alpha^{\rm 3D}_{\rm H}|$ in Fig. S5. As described in the main text, the reduction is recovered only by 10%, which means that the reduction of the spin diffusion length is not the main cause for the large reduction of the SH angle. We also obtain the same tendency using the 1D canculation.

We measured the I dependence of the ISHE and DSHE in $Cu_{98}Mn_{1.5}Bi_{0.5}$ at several different temperatures [see Fig. S6]. As references, the ISHE and DSHE in $Cu_{99.5}Bi_{0.5}$ are plotted in the same figures. Basically, there is little temperature dependence in $|\Delta R_{\rm SHE}|$ for $Cu_{99.5}Bi_{0.5}$. On the other hand, $|\Delta R_{\rm SHE}|$ of $Cu_{98}Mn_{1.5}Bi_{0.5}$ strongly depends on T [see

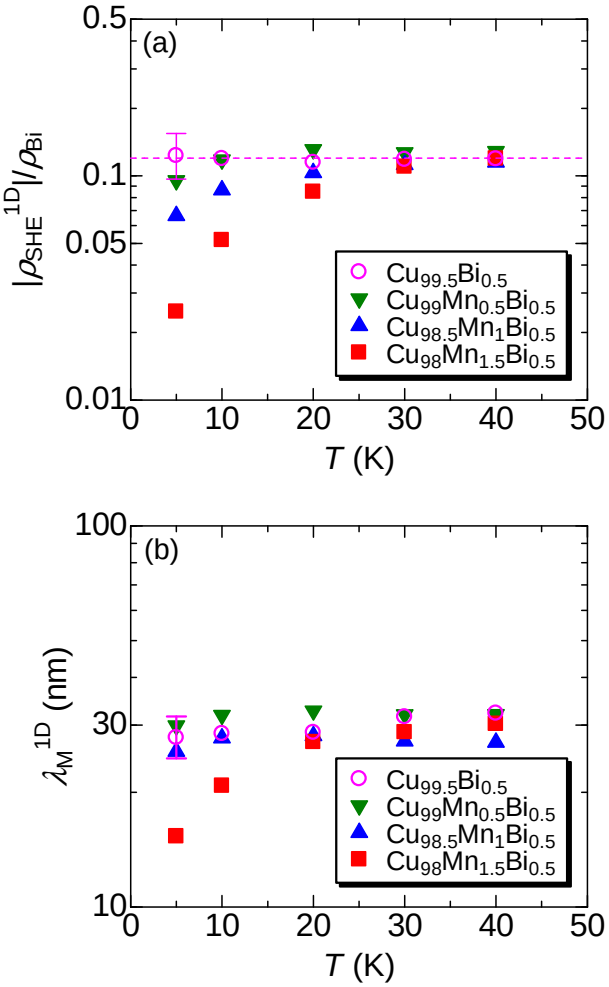

Figure S4: (a) SHE resistivities of CuMnBi $|\rho_{\rm SHE}^{\rm 1D}|$, obtained with the 1D calculation, divided by the resistivity induced by the Bi impurities $\rho_{\rm Bi}$ as a function of T. The broken line in the figure shows $|\alpha_{\rm H}^{\rm 1D}|$ of $Cu_{99.5}Bi_{0.5}$. (b) Spin diffusion lengths of CuMnBi $\lambda_{\rm M}^{\rm 1D}$ obtained with the 1D calculation as a function of T.

Fig. 2(e)]. As detailed in Ref. [16], the effective temperature of the SHE device depends on the injection current I because of the Joule heating in the Py wire. As a matter of fact, in the nonlocal geometry, it is not easy to estimate the effective device temperature. In Ref. [16], the charge imbalance effect at the interface between the Cu bridge and a superconducting Nb middle wire was used to calibrate the effective temperature at a certain I value.

In the present case, both ISHE and DSHE measurements have been used to check the effective temperature. The Onsager reciprocal relation, i.e., $\Delta R_{\rm DSHE} = \Delta R_{\rm ISHE}$ should be preserved in our device configuration [17]. However, in the case of CuMnBi, $\Delta R_{\rm DSHE} \neq$

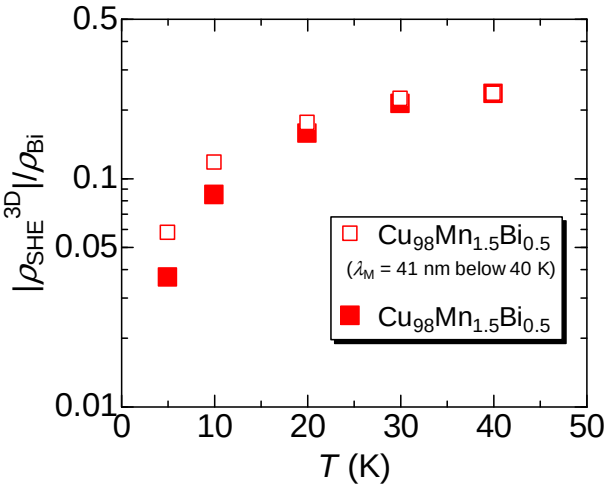

Figure S5: $|\rho_{\rm SHE}^{\rm 3D}|/\rho_{\rm Bi}$ of $Cu_{98}Mn_{1.5}Bi_{0.5}$ obtained with a constant $\lambda_{\rm M}^{\rm 3D}(= 41$ nm) below $T^* = 40$ K (open square). For comparison, $|\rho_{\rm SHE}^{\rm 3D}|/\rho_{\rm Bi}$ of $Cu_{98}Mn_{1.5}Bi_{0.5}$ shown in Fig. 3 is also plotted (closed square) in the same graph.

$\Delta R_{\rm ISHE}$ at larger I values. This is because the Joule heating effect is not equal for the two cases. At a sufficiently low I value, however, the Onsager relation is preserved. Thus, we have plotted $|\Delta R_{\rm SHE}|$ in Fig. 2(e) when $\Delta R_{\rm DSHE} = \Delta R_{\rm ISHE}$.

C. Extra data on AHE in CuMnIr

Using the same method as in Fig. 4, we have measured Hall resistivities ρ_{yx} of $Cu_{99-x}Mn_xIr_1$ ($x = 0$, 1, 3, and 6) and extracted only the anomalous part $d\delta\rho_{yx}/dH$. From the Curie law for $d\delta\rho_{yx}/dH$, one can determine the SH angle $\alpha_{\rm H}$ of CuIr (see the broken lines in the inset of Fig. S7). It is 0.018($\pm$0.003), which is again quantitatively consistent with previous measurements [12, 14, 20]. As in the case of CuMnBi, $d\delta\rho_{yx}/dH$ of CuMnIr starts to decrease at T^*, and it is shifted to the lower temperature side with decreasing the concentration of Mn. What is interesting to note is that $d\delta\rho_{yx}/dH$ of $Cu_{98}Mn_1Ir_1$ still follows a $1/T$ law down to 5 K, while $d\delta\rho_{yx}/dH$ of $Cu_{98.5}Mn_1Bi_{0.5}$ starts to deviate from the $1/T$ law at a much higher temperature. This fact clearly shows that the strength of the spin-orbit interaction of additionally added impurity (Bi or Ir) should play an important role in the reduction of $|\alpha_{\rm H}^{\rm 3D}|$ and in T^*. A similar discussion has been made in Refs. [21] and [22], based on the Dzyaloshinsky-Moriya interaction (DMI) between Mn via T (T: transition

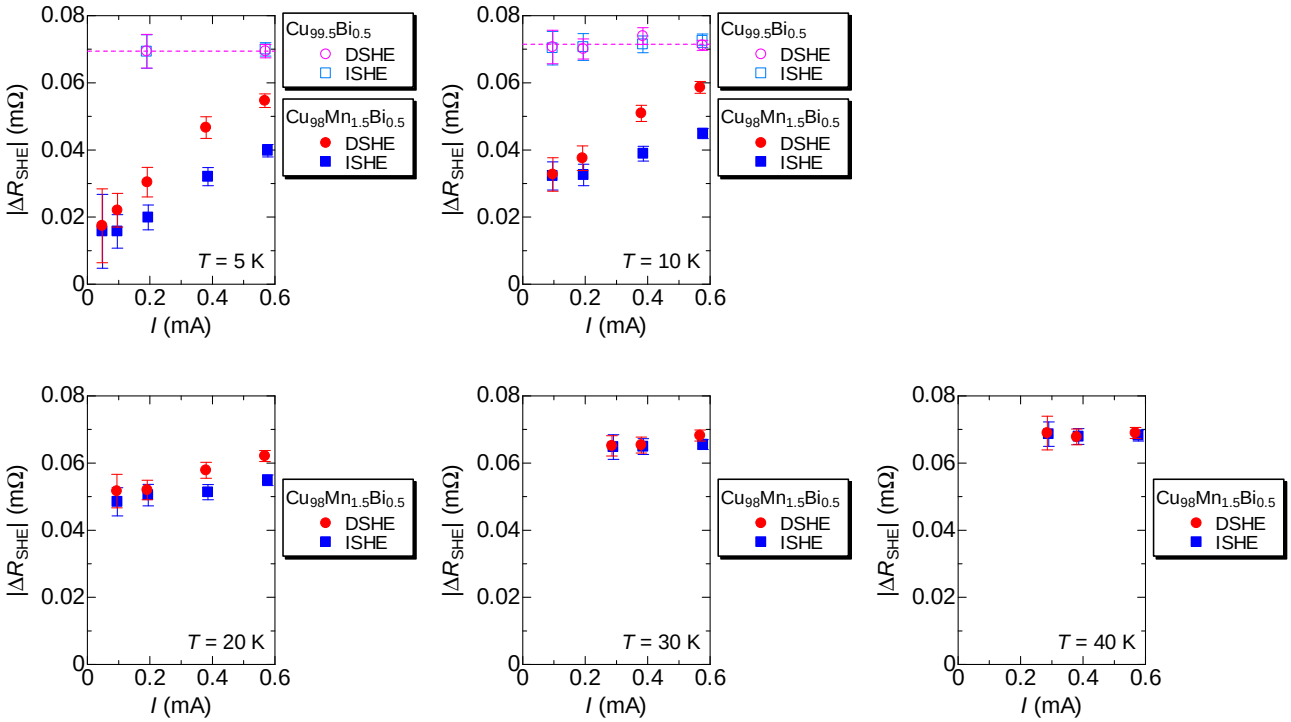

Figure S6: The I dependence of the ISHE and DSHE in $Cu_{98}Mn_{1.5}Bi_{0.5}$ at several different temperatures. For comparison, we also plot the I dependence of the ISHE and DSHE in $Cu_{99.5}Bi_{0.5}$ at 5 and 10 K.

metal), although the relation between the DMI and the large reduction of $|\alpha_{\rm H}^{\rm 3D}|$ is not clear at the moment.

We have also performed the SHE measurements with CuMnIr, but a clear reduction of $|\alpha_{\rm H}^{\rm 3D}|$ has not been observed even using $Cu_{93}Mn_6Ir_1$ whose spin glass temperature is exptected to be about 30 K [5]. This is probably because with 1% of Ir, $\Delta R_{\rm SHE}$ ($\sim 0.01{\rm m}\Omega$) is not large enough to see the clear reduction in the spin glass phase.

D. Kubo-Toyabe model to explain the large reduction of $|\alpha_{\rm H}|$

The model of Hayano *et al.* in Ref. [31] was developed as an analytically soluble model of a spin moment $\vec{s}$ precessing in a constant field $\vec{S}_0$ of magnitude ω_0/γ, taken in the z direction, plus a randomly fluctuating field $\vec{S}_{eff}(t)$. At each instant, the field $\vec{S}_{eff}(t)$ is uniformly distributed in direction, and has a magnitude defined by a Gaussian distribution

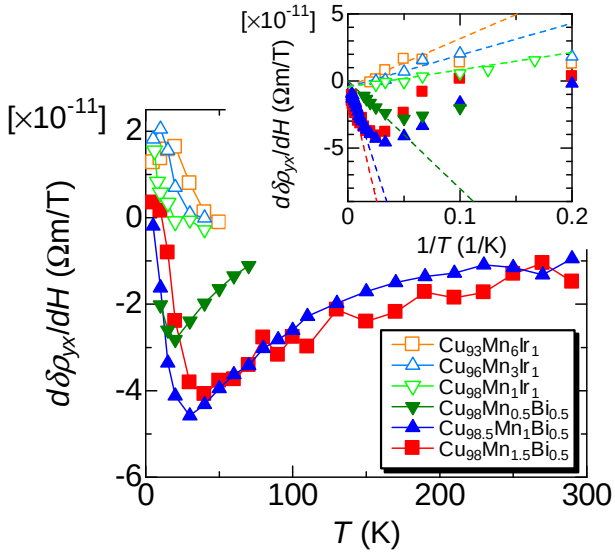

Figure S7: $d\delta\rho_{yx}/dH$ for $Cu_{99-x}Mn_xIr_1$ ($x = 0$, 1, 3, and 6) as a function of T. In the inset, they are plotted as a function of $1/T$. The broken lines show the linear fits to obtain $\alpha_{\rm H}$. For comparison, $d\delta\rho_{yx}/dH$ for $Cu_{99.5-x}Mn_xBi_{0.5}$ ($x = 0$, 0.5, 1, and 1.5) are also plotted (closed symbols) in the same graph.

P with a width of Δ:

$$P(\vec{S}_{eff}) = \frac{\gamma^3}{(2\pi)^{3/2}\Delta^3}\exp[-\frac{\gamma^2\vec{S}_{eff}^2}{2\Delta^2}].$$

If we first consider a *static* random field, the correlation function of $\vec{s}$ in the z direction, averaged over the field distribution, is given by the Gaussian integration:

$$g_z(t) =< s^z(0)s^z(t) >= 1 - \frac{2\Delta^2}{\omega_0^2}\left[1 - \exp\left(-\frac{1}{2}\Delta^2 t^2\right)\cos(\omega_0 t)\right] + \frac{2\Delta^4}{\omega_0^3}\int_0^t \exp\left(-\frac{1}{2}\Delta^2\tau^2\right)\sin(\omega_0\tau)d\tau.$$

$g_z(t)$ is known as the static Kubo-Toyabe function. In the "strong-collision" model [31], the random field $\vec{S}_{eff}(t)$ is given a special stochastic behavior: for each interval of time t, it retains a constant value with a probability $\exp(-\nu t)$, otherwise it has jumped to a statistically independent value from the same distribution. The correlation function $G_z(t,\nu)$ of the spin averaged over *all* time histories is then given by

$$G_z(t,\nu) = \sum_{n=0}^{\infty} g_z^{(n)}(t,\nu),$$

where $g_z^{(n)}(t,\nu)$ is the contribution from the histories, depending on the characteristic frequency ν, for which the field jumps exactly n times. For example, $g_z^0(t,\nu) = e^{-\nu t} g_z(t)$,

$$g_z^{(1)}(t,\nu) = \nu \int_0^\infty e^{-\nu(t-t_1)} g_z(t-t_1) e^{-\nu t_1} g_z(t_1) dt_1,$$

representing the history where there is a single jump at time t_1, and so forth. From the special property of the exponential, the Laplace transform of $G_z(t,\nu)$ is a geometric series of the Laplace transform $f_z(s) = \int_0^\infty g_z(t) e^{-st} dt$:

$$\int_0^\infty G_z(t,\nu) e^{-st} dt = \frac{f_z(s+\nu)}{1-\nu f_z(s+\nu)}.$$

By the inverse Laplace transform, the function $G_z(t,\nu)$ can be traced numerically, as shown in Fig. 3(a) in Ref. [31], for the case of a constant field $\omega_0 = 0$.

We have argued that the reduction of the skew scattered current will be $G_z(\tau_{\rm sk}, \nu(T))$ where the skew scattering time $\tau_{\rm sk}$ is defined by $\rho_{\rm SHE}^{\rm 3D} = \frac{m}{ne^2\tau_{\rm sk}}$ [32]. $\nu = \nu(T)$ is the frequency of correlation of the effective fields, which is large well above T_g, but will diminish to zero as the spin glass orders, as seen by both muons and neutrons [29]. This argument relies on the observation that the measured correlation times appear to be relatively independent of k-vector for the spin glass dynamics. We thus write the reduced spin Hall angle as

$$\alpha_{\rm CuMnBi}(T) = \alpha_{\rm CuBi} G_z(\tau_{\rm sk}, \nu(T)),$$

where $\alpha_{\rm CuBi}$ is the spin Hall angle from the Bismuth impurities alone.

We have taken a very simplified view in which there is critical slowing down with a power law of 2 [29] above the spin glass transition $\nu(T) = c(T-T_g)^2$ and for temperatures below T_g we consider just the frozen component: in other words, ν continues to vanish. A more complete model would have the effective field below the spin glass transition being a sum of a random static component depending on temperature and a dynamic component with varying the frequency. Even above T_g, our treatment is, for the moment, over-simplified; while the rate of exponential decay can vanish with critical slowing down, the correlation should cross over to a power law dependence. Nevertheless this gives a behavior for the spin Hall angle which looks reasonable. For the spin relaxation time τ_{sf}, we can take $(T_1)_{\rm Mn}$ from the asymptotic exponential decay of $G_z(t) \sim \exp[-t/(T_1)_{\rm Mn}]$ for $t \to \infty$ and

$$\frac{1}{\tau_{sf}} = \frac{1}{(T_1)_{\rm Mn}} + \frac{1}{\tau_{\rm Bi}},$$

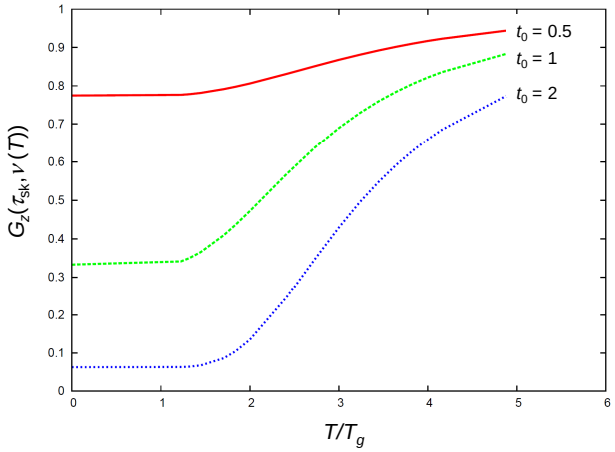

Figure S8: $G_z(\tau_{\rm sk}, \nu(T))$ as a function of temperature based on the Kubo-Toyabe model. The parameter t_0 is the dimensionless combination $\tau_{\rm sk}\Delta$. The scale of recovery to the high temperature value depends on the form taken for $\nu(T) \propto (T - T_g)^2$.

where $(T_1)_{\rm Mn}$ and $\tau_{\rm Bi}$ are the spin lattice relaxation time of Mn and the spin relaxation time due to the Bi impurities, respectively. This is reasonable in the motionally narrowed regime, but as we approach T_g, we probably need dissipation effects that are *not* included in the Kubo-Toyabe theory.

E. Theoretical discriptions on AHE

Detailed descriptions about how to evaluate the SH angle and the spin diffusion length with the SHE device have already been presented in Refs. [13] and [14]. Here we briefly review how to evaluate the SH angle from the AHE in CuMnBi(Ir) ternary alloys although more details can be seen in Appendix A of Ref. [20].

We follow the two-current model for spin-up ($\sigma =\uparrow$) and spin-down ($\sigma =\downarrow$) electrons formulated by Fert in Ref. [18]. The electric field can be written as

$$\begin{pmatrix} E_x^\sigma \\ E_y^\sigma \end{pmatrix} = \begin{pmatrix} \rho_{xx}^\sigma & -\rho_{yx}^\sigma \\ \rho_{yx}^\sigma & \rho_{xx}^\sigma \end{pmatrix} \begin{pmatrix} j_x^\sigma \\ j_y^\sigma \end{pmatrix}$$

where E_x^σ and E_y^σ are the detected electric fields along the x and y directions for spin σ, j_x^σ and j_y^σ are the incident electric current densities, and ρ_{xx}^σ and ρ_{yx}^σ are the longitudinal and transverse resistivities, respectively. For the AHE measurement, there is no incident

charge current in the y direction, i.e., $j_y^{\uparrow} + j_y^{\downarrow} = 0$. By combining with other two conditions, $E_x^{\uparrow} = E_x^{\downarrow} = E_x$ and $E_y^{\uparrow} = E_y^{\downarrow} = E_y$, one obtains

$$\rho_{yx}^{\mathrm{AHE}} \equiv \frac{E_y}{j_x^{\uparrow} + j_x^{\downarrow}} = \left(\frac{\rho_{xx}^{\downarrow}}{\rho_{xx}^{\uparrow} + \rho_{xx}^{\downarrow}}\right)^2 \rho_{yx}^{\uparrow} + \left(\frac{\rho_{xx}^{\uparrow}}{\rho_{xx}^{\uparrow} + \rho_{xx}^{\downarrow}}\right)^2 \rho_{yx}^{\downarrow}. \tag{S1}$$

In the present CuMnBi(Ir) ternary alloys, the Mn concentration is sufficiently low. When the interaction between the Mn impurities can be ignored, we have the following relation as in the case of nonmagnetic metals:

$$\rho_{yx}^{\uparrow} = -\rho_{yx}^{\downarrow} \equiv \rho_{yx}. \tag{S2}$$

By substituting Eq. (S2) into Eq. (S1), the simple equation can be derived:

$$\rho_{yx}^{\mathrm{AHE}} = \frac{\rho_{xx}^{\downarrow} - \rho_{xx}^{\uparrow}}{\rho_{xx}^{\uparrow} + \rho_{xx}^{\downarrow}} \rho_{yx} \equiv p\rho_{yx} \tag{S3}$$

where p is the spin polarization due to the Mn impurities.

We now formulate $\rho_{xx}^{\uparrow}$, $\rho_{xx}^{\downarrow}$, and ρ_{yx} in the CuMnBi(Ir) ternary alloys. Here we use the same method as in Ref. [20]. We start with the s-d Hamiltonian:

$$\mathcal{H} = (V_{\mathrm{Mn}} - J_{sd}\boldsymbol{\sigma} \cdot \boldsymbol{S}) \sum_i^{\mathrm{Mn}} \delta(\boldsymbol{r} - \boldsymbol{r}_i).$$

V_{Mn} is the impurity potential of Mn, J_{sd} is the s-d interaction due to the Mn impurity, $\boldsymbol{\sigma}$ (Pauli matrix) is the spin of conduction electron, $\boldsymbol{S}$ is the spin of Mn impurity, and $\boldsymbol{r}_i$ is the Mn impurity site. The matrix element can be expressed as

$$\langle \boldsymbol{k}, \sigma | \mathcal{H} | \boldsymbol{k}', \sigma' \rangle = V_{\mathrm{Mn}} \left(\delta_{\sigma,\sigma'} - \frac{J_{sd}}{V_{\mathrm{Mn}}} \boldsymbol{\sigma}_{\sigma,\sigma'} \cdot \boldsymbol{S}\right) \sum_i^{\mathrm{Mn}} e^{i\left(\boldsymbol{k}' - \boldsymbol{k}\right) \cdot \boldsymbol{r}_i}.$$

We note that J_{sd}/V_{Mn} is of the order of 0.1. Therefore, by solving the Boltzmann transport equation with the Born approximation and also by neglecting the correlation between the Mn impurities, the longitudinal resistivity due to the Mn impurities can be calculated as

$$\rho_{xx}^{\uparrow(\downarrow)}(\mathrm{Mn}) \approx \rho_{\mathrm{Mn}}^{*} \left[1 - (+)2\left(\frac{J_{sd}}{V_{\mathrm{Mn}}}\right) \langle S_z \rangle\right].$$

$\langle S_z \rangle$ is the exptected value of the z-component of Mn spin. Using the Matthiessen's rule, the longitudinal resistivity due to both Mn and Bi impurities can be written as

$$\rho_{xx}^{\uparrow(\downarrow)} \approx \rho_{\mathrm{Mn}}^{*} \left[1 - (+)2\left(\frac{J_{sd}}{V_{\mathrm{Mn}}}\right) \langle S_z \rangle\right] + \rho_{\mathrm{Bi}}^{*}. \tag{S4}$$

It should be noted that ρ^*_{Mn} and ρ^*_{Bi} are different from normal resistivities, ρ_{Mn} and ρ_{Bi}. This has also been pointed out by Fert and Levy in their recent paper (see Ref. [19]). Since the total longitudinal resistivity ρ_{xx} is $\rho^{\uparrow}_{xx}\rho^{\downarrow}_{xx}/\left(\rho^{\uparrow}_{xx}+\rho^{\downarrow}_{xx}\right)$, the normal resistivities of Mn (ρ_{Mn}) and Bi (ρ_{Bi}) can be expressed as

$$\rho_{\mathrm{Mn}} \approx \frac{\rho^*_{\mathrm{Mn}}}{2}, \tag{S5}$$

$$\rho_{\mathrm{Bi}} = \frac{\rho^*_{\mathrm{Bi}}}{2}, \tag{S6}$$

respectively. By substituting Eqs. (S4)-(S6) into Eq. (S3), one obtains

$$\begin{aligned}\rho^{\mathrm{AHE}}_{yx} &= \left[2\left(\frac{\rho_{\mathrm{Mn}}}{\rho_{\mathrm{Mn}}+\rho_{\mathrm{Bi}}}\right)\left(\frac{J_{sd}}{V_{\mathrm{Mn}}}\right)\langle S_z\rangle\right]\rho_{yx} \\ &= \left[2\left(\frac{\rho_{\mathrm{Mn}}\rho_{\mathrm{Bi}}}{\rho_{\mathrm{Mn}}+\rho_{\mathrm{Bi}}}\right)\left(\frac{J_{sd}}{V_{\mathrm{Mn}}}\right)\langle S_z\rangle\right]\alpha_{\mathrm{H}}. \end{aligned} \tag{S7}$$

In Eq. (S7), α_{H} is defined as $\rho_{yx}/\rho_{\mathrm{Bi}}$ since Bi is only the skew scatterer in the ternary alloy.

In the low magnetic field limit (i.e., $\mu_{\mathrm{B}}H \ll k_{\mathrm{B}}T$), we can write

$$\langle S_z\rangle = \frac{g\mu_{\mathrm{B}}S(S+1)H}{3k_{\mathrm{B}}T}$$

where g, μ_{B}, S, and k_{B} are the g-factor, the Bohr magneton, the magnitude of the spin, and the Boltzmann constant, respectively. For Mn impurities in Cu, $g = 2$ and $S = 2$ [20]. As mentioned above, $J_{sd}/V_{\mathrm{Mn}} = 0.133$ [20]. When the interaction between Mn impurities can be neglected, $d\rho^{\mathrm{AHE}}_{yx}/dH$ simply follows a $1/T$ law, and thus α_{H} can be evaluted from the slope of $d\rho^{\mathrm{AHE}}_{yx}/dH$ vs $1/T$ as shown in the inset of Fig. 4(b). We have already known that $\rho_{\mathrm{Bi}} = 5.1$ $\mu\Omega$·cm for Bi 0.5% [13] and $\rho_{\mathrm{Ir}} = 3.1$ $\mu\Omega$·cm for Ir 1% [12]. By putting all the values in Eq. (S7), we obtain $\alpha_{\mathrm{H}} = -0.23(\pm 0.06)$ for CuMnBi and $\alpha_{\mathrm{H}} = 0.018(\pm 0.003)$ for CuMnIr. The SH angles estimated with this method are quantitatively consistent with those determined with the SHE devices [12, 13]. It should be noted that since this method relies on the $1/T$ law, the SH angle below T^* cannot be determined quantitatively.